International Journal of Science and Research (IJSR)
ISSN (Online): 2319-7064
Impact Factor (2012): 3.358

Digital Modulation Characteristics of Violet InGaN Laser Diodes with Ternary AlGaN and Quaternary AlInGaN Blocking Layers

Rafid A. Abdullah[1] , Kamarulazizi Ibrahim[2]

[1]Science College, University of Mosul, Mosul, Iraq

[2]School of Physics, Universiti Sains Malaysia,11800 Penang, Malaysia

Abstract: ***The outputs of the MQW violet InGaN laser diode (LD) with ternary AlGaN blocking layer (BL) (LD1) and quaternary AlInGaN BL (LD2) have been analyzed and the parameters of LDs have been calculated. Coupling ISE TCAD simulator with MATLAB program has been proposed and utilized to simulate the digital modulation of the LDs. Several operating points on L-I curves of LD1 and LD2 have been selected and examined of pulse response for the purpose of the direct digital modulation investigation. The simulation results indicated that LD2 has relatively lower relaxation oscillation (RO) and higher frequency of RO than LD1. The bit rate, turn-on and turn-off times, and extinction ratio have been investigated and calculated from pulse responses of LD1 and LD2. The maximum bit rate calculated of MQW violet InGaN LDs was 500 Gb/s. In general, it was found that LD2 is better than LD1 for direct digital modulation behavior due to its lower RO, K ratio (photon lifetime/carrier lifetime), damping constant and higher frequency of RO than LD1. Parameters calculated and direct digital modulation results presented in this work are in line with related experimental studies.***

Keywords: Digital modulation, Quaternary AlInGaN, Blocking layer, InGaN laser diode

1. Introduction

Group III-nitride materials have been recognized as one of the most promising optoelectronic semiconductor materials because they possess excellent mechanical properties such as high melting point, high hardness, and high thermal conductivity. In addition, group III-nitride materials have large direct tunable band gaps which are appropriate for short-wavelength LEDs and LDs where the usefulness and goodness of GaN and its alloys have been well established for the fabrication from visible to ultraviolet (UV) LEDs and LDs.

Violet LD that is based on these materials, especially the LD with an emission wavelength near 405 nm has attracted great interest as a light source for high-density optical data storage, high-resolution color printing, chemical sensor, medical applications, and undersea optical communication systems.

Since the demonstration of the first InGaN/GaN LD by Nakamura et al. [1], significant progress has been made towards reducing the threshold current, increasing the output power, increasing the lifetime of the LDs and improving the device characteristics.

The quaternary $Al_xIn_yGa_{1-x-y}N$ alloy is potential for the fabrication of lattice matched III-nitride by independently controlling the band gap energy and the lattice constant and it has better lattice match to GaN resulting in a decrease of dislocations [2, 3]. Moreover, the use of $Al_xIn_yGa_{1-x-y}N$ quaternary materials is proved to be a promising approach in realizing deep UV devices [4].

The growth temperature of quaternary AlInGaN by metal organic chemical vapor deposition (MOCVD) ranges from 750 to 900 ^oC [2, 5, 6]; and this is close to the growth temperature of the InGaN active region. As a result, this makes the indium prevention by evaporation from the InGaN active region better when using it as a blocking layer (BL) than using the conventional ternary AlGaN BL.

Theoretically, J. R. Chen et al. showed that the built-in polarization can be reduced by using quaternary AlInGaN as a BL instead of ternary AlGaN BL [7]. The optical properties of InGaN MQW LDs with different polarization-matched AlInGaN barrier layers have been investigated numerically by S. Park et al. [8]. These researchers showed that the use of quaternary polarization-matched AlInGaN barrier layers enhances the electron-hole wavefunction overlap due to the compensation of polarization charges between InGaN QW and AlInGaN barrier layer. The optimal polarization-matched InGaN/AlInGaN LD showed lower threshold current and higher slope efficiency compared to the conventional $In_xGa_{1-x}N/In_yGa_{1-y}N$ LDs. C. Skierbiszewski et al. used the quaternary AlInGaN in the superlattice cladding layer of the LD as AlInGaN/InGaN pairs instead of conventional AlGaN/GaN pairs; they relatively obtained high output power (60 mW) at room temperature [9]. On the other hand, Wei Yang et al. have theoretically shown that the InGaN LD performance can be enhanced by using tapered and graded AlGaN BL [10].

The InGaN LDs near 405 nm are expected to play an important role in undersea optical communication systems, especially after increasing their lifetimes where long lifetime is always needed for laser used in optical communication systems. Moreover, the digital modulation of the pulse response of violet InGaN LDs is also required in other

applications. Therefore, the analysis of digital modulation and pulse response of violet InGaN LD are required to examine the ability of this laser to build a clean square wave of pulse response. The other items of the digital modulation of violet InGaN LD such as RO, turn-on and turn-off times, and bit rate have not been sufficiently clarified yet.

However, there is very little information about the digital modulation of violet InGaN LDs. The violet InGaN LDs have been modulated with pulse current in order to measure the carrier lifetime experimentally by S. Nakamura et al. and M. Kuramoto et al. [11,12]. M. Kuramoto et al. studied the relationship between the slope gain and frequency of the relaxation oscillation of the violet InGaN LDs with emission wavelengths at 411, 404 and 397 nm. They observed the ROs in the pulse response for these three LDs and concluded that the LD which has higher RO, also has a higher carrier lifetime [12]. S. Nakamura et al. modulated the MQW violet InGaN LD with an emission wavelength near 405 nm, and they measured the frequency of the RO which was 3 GHz [13].

In this paper, the digital modulation characteristics of MQW InGaN violet LDs with ternary and quaternary BLs are theoretically investigated by coupling MATLAB with ISE-TCAD simulation program.

2. Theoretical Framework

The LD dynamic behaviors are modeled by a set of two time-dependent differential equations which describe the relationship between the carrier density $N(t)$ and the photon density $S(t)$ together with the optical phase $\Phi(t)$ [14]:

$$\frac{dN(t)}{dt} = \frac{I(t)}{q \cdot v_a} - g_o \frac{[N(t) - N_o] \cdot S(t)}{1 + \varepsilon \cdot S(t)} - \frac{N(t)}{\tau_n} \quad (1)$$

$$\frac{dS(t)}{dt} = \Gamma \cdot g_o \frac{[N(t) - N_o] \cdot S(t)}{1 + \varepsilon \cdot S(t)} - \frac{S(t)}{\tau_p} + \frac{\Gamma \cdot \beta}{\tau_n} \cdot N(t) \quad (2)$$

$$\frac{d\Phi(t)}{dt} = \frac{1}{2}\alpha \left[\Gamma \cdot g_o [N(t) - N_o] - \frac{1}{\tau_p} \right] \quad (3)$$

where Γ is the optical confinement factor which describes how much mode is confined in the active region, N_o is the carrier density at transparency for which the net gain is zero, τ_p is the average photon lifetime inside the cavity, τ_n is the carrier lifetime, $I(t)$ is the injection current, β is the fraction of the spontaneous emission that couples with the lasing mode, q is the electron charge, v_a is the active region volume which can be omitted if the equations are to be interpreted in terms of carrier and photon numbers, g_o is the slope gain constant, α is the linewidth enhancement factor and ε is the gain compression factor or non-linear gain coefficient.

These are large signal single-mode rate equations that describes the LD behavior in both spontaneous emission and stimulated emission regions as it can be viewed in Figure 1 which represents the full operating regions of the LD. From the equations above, it is possible to derive a set of steady-state and small signal equations to help in further understanding the static and dynamic behaviors of LDs.

The rate equations are used to describe the output optical power versus input current, the modulation response to the sinusoidal bias current, and the operating characteristics for laser amplifiers. Moreover, a numerical optimization technique is employed to extract the rate equation parameters of the LDs where all parameters can be extracted in a self-consistent manner [15].

The nonlinearity in the LD behaviors is due to the spontaneous emission coupled into lasing mode, mirror reflectivities, internal parameters, leakage current, axial hole burning, and temperature variations [16]. Therefore, this nonlinearity behavior of the LD is expressed by non-linear gain coefficient (ε) as well as spontaneous emission factor (β).

If the regime of the stimulated emission is kink-free, this means that the LD operates with fundamental single transverse mode. If it is not kink-free, this means that the LD operates with more than one transverse mode where the kink is due to the transition of one transverse-mode to another.

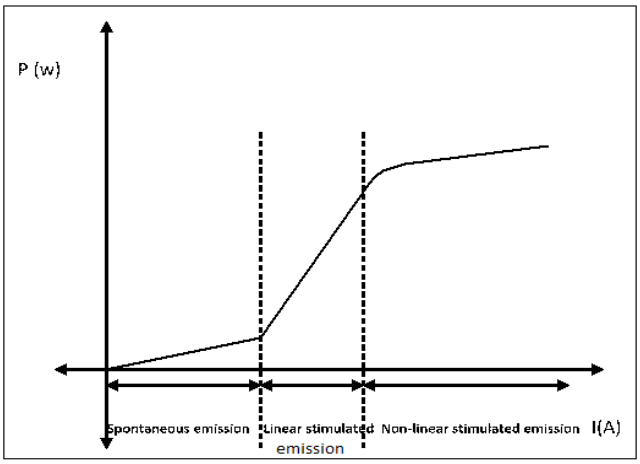

Figure 1: Full operating regions of the laser diode.

For the arbitrary operating points that are close to the threshold current, gain saturation term $1/(1+\varepsilon.S(t))$ will be approximated to 1 for the value of $\varepsilon.S(t)<<1$. This term will have negligible effect on Eq. (1) and Eq. (2).

Building a signal model is essential in determining operating points within the 'semi' linear lasing region. In these operating points, the lasing region which is defined above threshold current, are used to characterize the small signal response [102]. The process of selecting the operating point is as follows: choose an arbitrary operating point close to the threshold current. Therefore, the gain saturation term $1/(1+\varepsilon.S(t))$ will be approximated to 1 for values of $\varepsilon.S(t)<<1$. This term will have negligible effect on Eq. (1) and Eq. (2). Figure 2 shows the principle of selecting an operating point. Hence according to [17] partial derivatives with respect to $N(t)$ and $S(t)$ can safely be taken as:

$$\frac{\partial\left(\frac{dN(t)}{dt}\right)}{\partial N(t)} = -\frac{1}{\tau_n} - g_o \cdot S(t) \quad (4)$$

$$\frac{\partial\left(\frac{dN(t)}{dt}\right)}{\partial S(t)} = -g_o \cdot [N(t) - N_o] \quad (5)$$

$$\frac{\partial\left(\frac{dS(t)}{dt}\right)}{\partial N(t)} = \Gamma \cdot g_o \cdot S(t) + \frac{\Gamma \cdot \beta}{\tau_n} \quad (6)$$

$$\frac{\partial\left(\frac{dS(t)}{dt}\right)}{\partial S(t)} = \Gamma \cdot g_o \cdot [N(t) - N_o] - \frac{1}{\tau_p} \quad (7)$$

The state-space model of couple rate equations is:

$$\begin{bmatrix} \dot{N} \\ \dot{S} \end{bmatrix} = A \begin{bmatrix} N \\ S \end{bmatrix} + Bf(t) \quad (8)$$

$$y = C \begin{bmatrix} N \\ S \end{bmatrix} + Df(t) \quad (9)$$

The first row of *A* and the first row of *B* are the coefficients of the first rate equation for $\frac{dN(t)}{dt}$. Likewise, the second row of *A* and the second row of *B* are the coefficients of the second rate equation for $\frac{dS(t)}{dt}$. *C* and *D* are the coefficients of the output equation for *y* where *y* is the desired output for the photon density. Jacobian matrix in state-space model will be applied as in the following equations:

$$\begin{bmatrix} \dot{N} \\ \dot{S} \end{bmatrix} = \begin{bmatrix} \frac{\partial\left(\frac{dN(t)}{dt}\right)}{\partial N(t)} & \frac{\partial\left(\frac{dN(t)}{dt}\right)}{\partial S(t)} \\ \frac{\partial\left(\frac{dS(t)}{dt}\right)}{\partial N(t)} & \frac{\partial\left(\frac{dS(t)}{dt}\right)}{\partial S(t)} \end{bmatrix} \cdot \begin{bmatrix} N \\ S \end{bmatrix} + \begin{bmatrix} \frac{1}{qV_a} \\ 0 \end{bmatrix} \cdot I(t) \quad (10)$$

$$y = \begin{bmatrix} 0 & 1 \end{bmatrix} \cdot \begin{bmatrix} N \\ S \end{bmatrix} \quad (11)$$

By substituting Eqs. (4-7) into Eq. (10), we can obtain [17]:

$$\begin{bmatrix} \dot{N} \\ \dot{S} \end{bmatrix} = \begin{bmatrix} -\frac{1}{\tau_n} - g_o.S(t) & -g_o.[N(t) - N_o] \\ \Gamma.g_o.S(t) + \frac{\Gamma.\beta}{\tau_n} & \Gamma.g_o.[N(t) - N_o] - \frac{1}{\tau_p} \end{bmatrix} \cdot \begin{bmatrix} N \\ S \end{bmatrix} + \begin{bmatrix} \frac{1}{qV_a} \\ 0 \end{bmatrix} .I(t) \quad (12)$$

$$y = \begin{bmatrix} 0 & 1 \end{bmatrix} \cdot \begin{bmatrix} N \\ S \end{bmatrix} \quad (13)$$

Therefore,

$$A = \begin{bmatrix} -\frac{1}{\tau_n} - g_o.S(t) & -g_o.[N(t) - N_o] \\ \Gamma.g_o.S(t) + \frac{\Gamma.\beta}{\tau_n} & \Gamma.g_o.[N(t) - N_o] - \frac{1}{\tau_p} \end{bmatrix} \quad (14)$$

$$B = \begin{bmatrix} N \\ S \end{bmatrix} \quad (15)$$

$$C = \begin{bmatrix} 0 & 1 \end{bmatrix} \quad (16)$$

$$D = \begin{bmatrix} 0 \end{bmatrix} \quad (17)$$

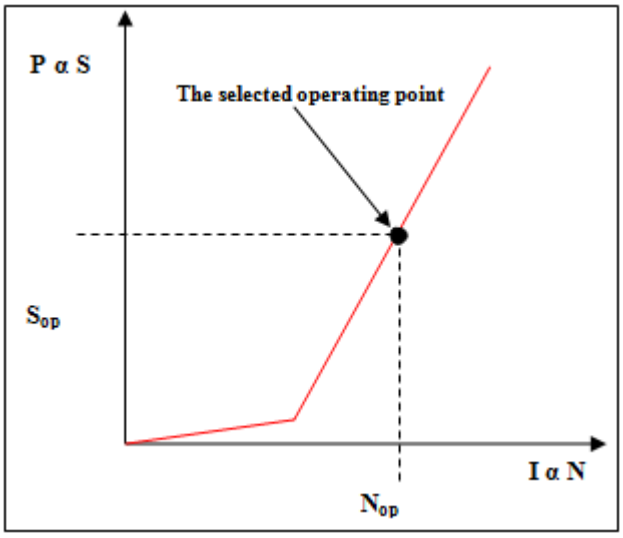

Figure 2: The principle of selecting an operating point

3. MQW violet InGaN Laser Diode Structure Under Study

In general, the schematic diagram of MQW violet InGaN LD under study is similar to Nakamura's design structures [1, 18, 19]. Therefore, this design structure refers to a real structure grown in laboratory. Because Nakamura's experimental studies have proved that the violet InGaN LD with double quantum well (DQW) has the best properties [18-20], this study focus on the DQW (active region) as a based design structure. Because the quaternary AlInGaN BL will be considered in this study, the thickness of BL has been chosen as 14 nm based on the study conducted by C. Skierbiszewski et al. [21]. A schematic diagram of the preliminary MQW violet InGaN LD structure under study is shown in Figure 3. In this simulation, it is assumed that the MQW violet InGaN LD is grown on the n-type GaN layer whose thickness is 2 µm. On the top of this GaN layer is a 0.1- µm-thick n-type $In_{0.05}Ga_{0.95}N$ compliance layer and a 0.48- µm-thick n-type $Al_{0.07}Ga_{0.93}N$ cladding layer, followed by a 0.1-µm-thick n-type GaN guiding layer. The active region consists of double $In_{0.12}Ga_{0.88}N$ undoped QWs where the thickness of every well is 2.5 nm, and every well is sandwiched between two 5-nm-thick $In_{0.01}Ga_{0.99}N$ barriers. A 14 -nm-thick p-type

$Al_{0.18}Ga_{0.82}N$ or AlInGaN BLs is grown on top of the active region, followed by a 0.1-μm-thick p-type GaN guiding layer and a 0.48-μm-thick p-type $Al_{0.07}Ga_{0.93}N$ cladding layer. Finally, a 0.1-μm-thick p-type GaN cap layer is grown over p-type cladding layer to complete the structure. The doping concentrations of n-type and p-type are equal to 1×10^{18} and 5×10^{18} cm^{-3}, respectively. The band offset ratio, which is defined as the ratio between the conduction band offset and the valence band offset ($\Delta E_c / \Delta E_v$) of $In_xGa_{1-x}N$ / $In_yGa_{1-y}N$ QW, is assumed to be 0.7/0.3. The active region is 1 μm in width and 750 μm in length. The reflectivities of the two end facets were assumed to be 50% for each one for lower threshold current density as Nakamura concluded in his design [19].

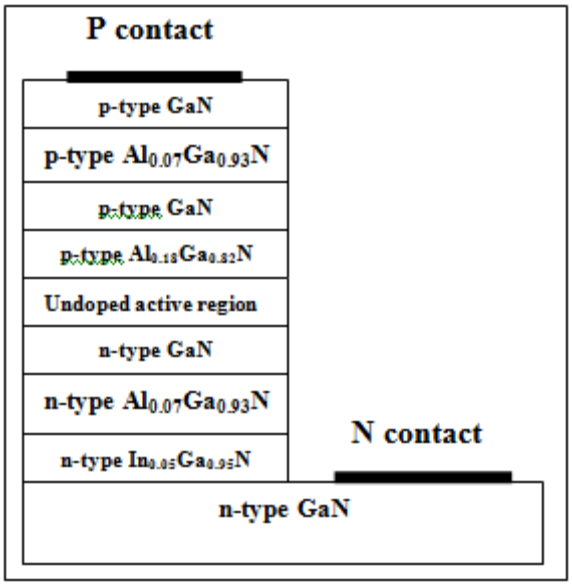

Figure 3: A schematic diagram of the preliminary MQW violet InGaN LD structure under study.

The values of all LD parameters, which were calculated and required for the study and analysis of the pulse response of digital modulation of the LD1 and LD2, are listed in Table 1.

Table 1: The parameters of LD1 and LD2

Parameter	*Value of LD1*	*Value of LD2*	*Unit*
Active region volume	1.5×10^{-11}	1.5×10^{-11}	cm^3
Carrier density at threshold	1.66×10^{19}	1.32×10^{19}	cm^{-3}
Carrier density at transparency	1.367×10^{19}	1.067×10^{19}	cm^{-3}
Carrier lifetime	2.43×10^{-9}	2.3×10^{-9}	s
Differential quantum efficiency	0.487	0.5	
Internal loss	9.35	8.05	cm^{-1}
Internal quantum efficiency	92	94	%
Laser cavity length	0.075	0.075	cm
Mirror loss	9.24	9.24	cm^{-1}
Photon lifetime	4.48×10^{-12}	4.82×10^{-12}	s
Optical confinement factor	0.0075	0.008	
Slope gain constant	1×10^{-5}	1×10^{-5}	$cm^{-3}.s^{-1}$
Spontaneous emission factor	0.68×10^{-5}	0.72×10^{-5}	
Threshold current	16.42	13.76	mA
Threshold current density at transparency	1800	1485	A/cm^2
Threshold gain	18.587	17.29	cm^{-1}
Wavelength	406.66	406.66	nm

4. Selecting the operating points

The operating points required for the study and analysis of the pulse responses of two LD designs for digital modulation are selected. Five operating points for each design are selected. These points should be slightly above the threshold current for two reasons. The first reason is because of the use of the approximation $\varepsilon.S(t)<<1$ in rate equations when Jacobian matrix was applied in state-space. The second reason, in optical communication systems, the bias LD is always slightly above the threshold current to avoid the unwanted relaxation oscillation. Consequently, the study and analysis of the pulse response in this area are very important.

The powers with the corresponding currents of the selected operating points are extracted from L-I curves of the two designs. Figure 4 and Figure 5 represent the selected operating points which will be used to study and analyze the pulse response for digital modulation of both designs. Only part of the L-I curves of LD1 and LD2 near threshold current have been considered. The selected operating points of LD1 are included in Table 2 and the selected operating points of LD2 are included in Table 3.

Table 2: Selected operating points of LD1.

Current (mA)	*Power (mW) per facet*	*Carrier density* $(cm^{-3}) \times 10^{19}$	*Photon density* $(cm^{-3}) \times 10^{13}$
17	0.27	1.66	0.508
17.5	0.515	1.66	0.969

18	0.8	1.66	1.5054
18.5	1.1	1.66	2.07
19	1.4	1.66	2.6345

Table 3: Selected operating points of LD2.

Current (mA)	*Power (mW) per facet*	*Carrier density* $(cm^{-3}) \times 10^{19}$	*Photon density* $(cm^{-3}) \times 10^{13}$
14	0.25	1.32	0.525
14.5	0.55	1.32	1.1569
15	0.87	1.32	1.83
15.5	1.2	1.32	2.524
16	1.54	1.32	3.05

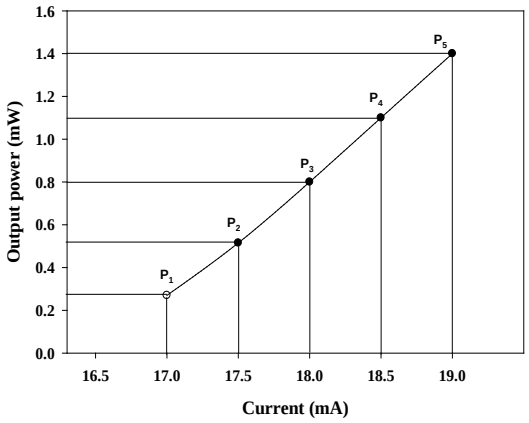

Figure 4: Selected operating points of LD1.

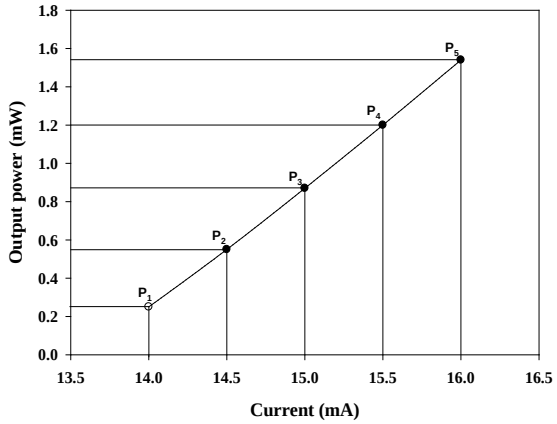

Figure 5: Selected operating points of LD2.

5. Pulse response and relaxation oscillation of MQW violet InGaN LDs

Most LD systems modulate the output beam by modulating the bias current of the LD. Therefore, it is needful to have a sufficient knowledge of its pulse response to the input current where the input current (I_{ip}) in the LD is assumed to consist of a bias current (I_b) and a modulation current (I_m), as:

$I_{ip}=I_b+I_m(t)$ (18)

The bias current is a constant current that pushes the LD operating beyond the threshold current value and into the linear region. The modulation current is an alternative current that is switched on and off in synchronization with the input current waveform. In fact, one of the factors which limit the data rate is the switching speed of the LD. For the fast switching operating, it is common to bias the LD slightly above the threshold current to avoid turn-on delay time [22].

The relaxation oscillation (RO) is always coupled with the pulse response of LD. Because most LDs are working under class B in which the carrier lifetime (τ_n) is longer than the photon lifetime (τ_p), the RO is expected to appear in the pulse response.

The LDs under study are modulated with 1 mA above the operating points whose details are described in Tables 2 and 3. The injected modulation signal starts at zero ns and ends at 12 ns with duration of 3 ns.

Firstly, the pulse responses and ROs of digital modulation of LD1 are investigated. Figure 6 shows the input current to the LD1, it is equal to the bias current plus modulation current (square wave). Figure 7 shows the pulse response of LD1 at the bias operating point of 17 mA. The overshoot appears on the pulse response due to the RO, and the RO is due to the interaction between the electrons and photons. Therefore, when the interaction between the electrons and photons increases the RO also increases. The ROs are expected to increase due to the increase of the photon density of the LD when increasing the bias current of the LD as it can be seen in Figures (8-11) where these figures represent the pulse responses of the LD1 at 17.5, 18, 18.5 and 19 mA, respectively.

Secondly, pulse responses and the ROs for digital modulation of LD2 are investigated. Figure 12 shows the input current to the LD2, it is equal to the bias current plus modulation current (square wave). Figure 13 shows the pulse response of LD2 at the bias operating point of 14 mA. The overshoot also appears on the pulse response due to the RO. When increasing the bias points above the threshold current, the RO in the pulse response increases due to the increase of the interaction between the electrons and photons. Figure (14-17) represent the pulse responses of the LD2 at 14.5, 15, 15.5 and 16 mA, respectively.

By comparison between the RO of LD1 and LD2, one can see that the ROs of LD2 is slightly lower than the ROs of LD1. This result can be discussed with *K* ratio which is equal to $\frac{\tau_n}{\tau_P}$ where the RO mainly depends on the carrier lifetime (τ_n) and photon lifetime (τ_p). The LD does not generate the RO when the ratio of $K \leq 1$ [23]; hence, when the *K* ratio is low, the RO is also low. *K* ratio of LD1 is 542.4 and *K* ratio of LD2 is 477.2. On the other hand, the damping of RO, which is called the damping constant, also plays a role in reducing the ROs in LD2. The damping constant is given approximately by $2\tau_n$ [24], and it was found to be 4.86 and 4.6 ns of LD1 and LD2, respectively. This slightly difference between these two values of damping constants also makes the ROs of LD2 lower than that of LD1.

Based on the simulation results of this study, although there is a slight difference in the pulse response behaviors between LD1 and LD2, it can be concluded that the LD2 is better than

LD1 for digital modulation where reducing the RO of LD is the ultimate goal for optical communication systems.

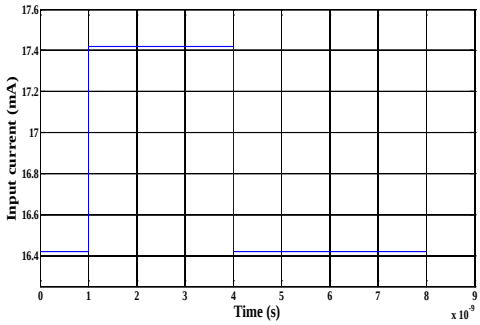

Figure 6: The input current to the LD1, it is equal to the bias current plus modulation current (square wave).

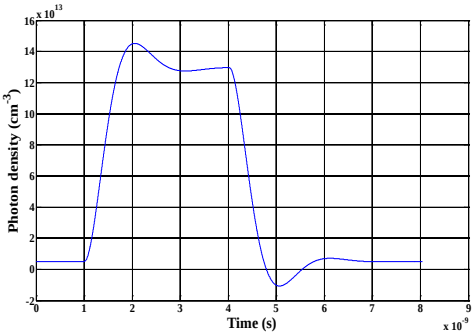

Figure 7: The pulse response to 3 ns with 1 mA modulation current at the bias operating point of 17 mA of LD1.

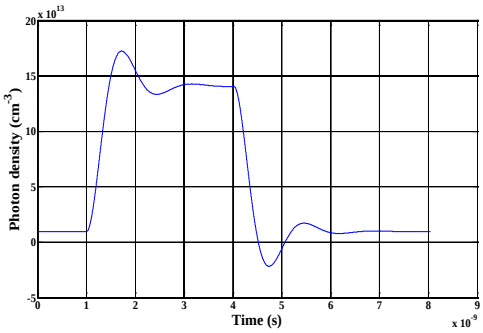

Figure 8: The pulse response to 3 ns with 1 mA modulation current at the bias operating point of 17.5 mA of LD1.

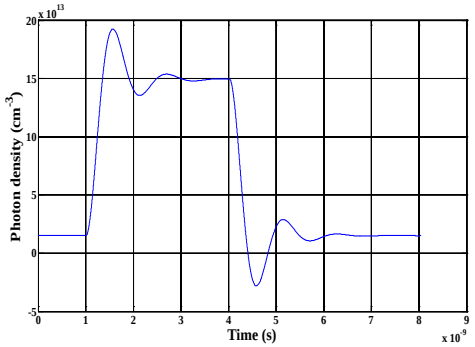

Figure 9: The pulse response to 3 ns with 1 mA modulation current at the bias operating point of 18 mA of LD1.

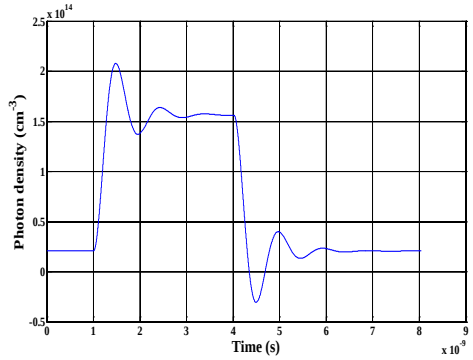

Figure 10: The pulse response to 3 ns with 1 mA modulation current at the bias operating point of 18.5 mA of LD1.

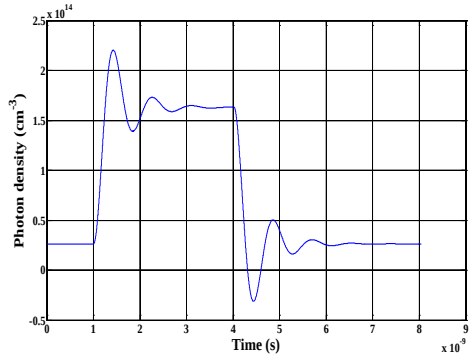

Figure 11: The pulse response to 3 ns with 1 mA modulation current at the bias operating point of 19 mA of LD1.

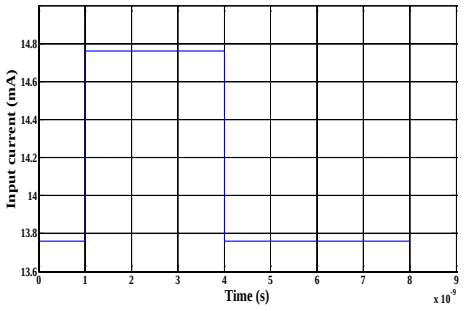

Figure 12: The input current to the LD2, it is equal to the bias current plus modulation current (square wave).

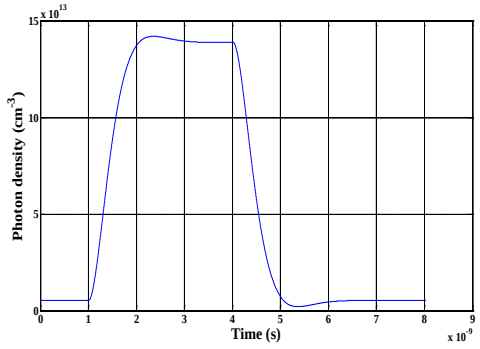

Figure 13: The pulse response to 3 ns with 1 mA modulation current at the bias operating point of 14 mA of LD2.

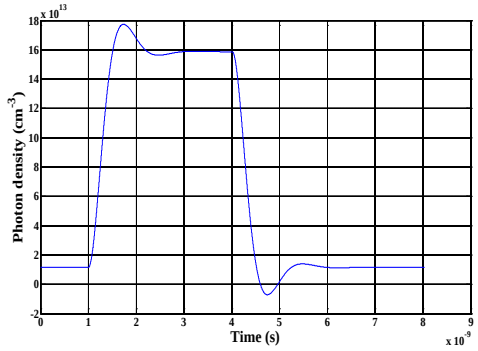

Figure 14: The pulse response to 3 ns with 1 mA modulation current at the bias operating point of 14.5 mA of LD2.

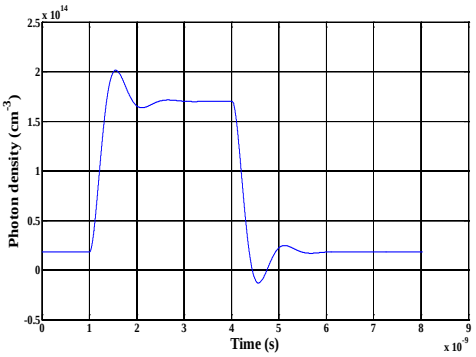

Figure 15: The pulse response to 3 ns with 1 mA modulation current at the bias operating point of 15 mA of LD2.

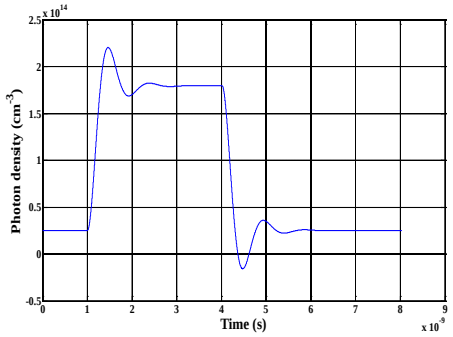

Figure 16: The pulse response to 3 ns with 1 mA modulation current at the bias operating point of 15.5 of LD2. .

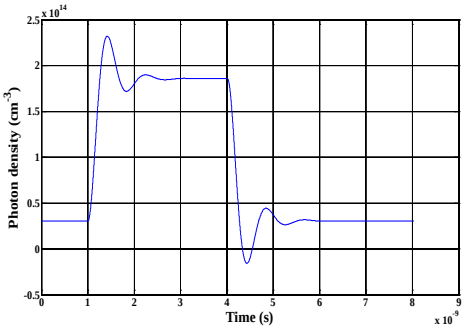

Figure 17: The pulse response to 3 ns with 1 mA modulation current at the bias operating point of 16 mA of LD2.

K ratio in typical conventional LDs is approximately 1000 where the carrier lifetime is around 3 ns and the photon lifetime is around 1 ps, especially in LDs which are used in optical communication systems such as quantum well - distributed feedback (QW-DFB) LD. To compare between MQW violet InGaN LDs under study and the conventional QW-DFB LD, the pulse response of the QW-DFB LD will be presented in a suitable scale. The parameters required for the QW-DFB LD were taken from reference [22]. The carrier density and photon density of the QW-DFB LD above the threshold current at 5.68 mA were taken from reference [17]. Therefore, the LD1 and LD2 are modulated above their threshold currents at 5.68 mA. 0

Figure 18 shows the pulse response of LD1at the bias operating point of 22.1 mA, Figure 19 shows the pulse response of LD2 at the bias operating point of 19.44 mA and Figure 20 shows the pulse response of QW-DFB LD at the bias operating point of 15 mA where the threshold currents are 16.42, 13.76 and 9.32 mA for the LD1, LD2 and QW-DFB LD, respectively; and that the duration currents of these pulse responses are 3 ns.

It is obvious from these three figures that the RO of QW-DFB LD is higher than the ROs of LD1 and LD2. This is because *K* ratio of the QW-DFB is 1000 and this value is almost twice higher than *K* ratio of LD1 and LD2. From Figure 19 and Figure 20, one can see that the RO of the pulse response of LD2 is slightly lower than that of LD1 as discussed earlier. On the other hand, the damping constants for LD1, LD2 and QW-DFB LD are 4.86 ns, 4.6 and 6 ns, respectively. The higher damping constant of QW-DFB LD also increases the RO.

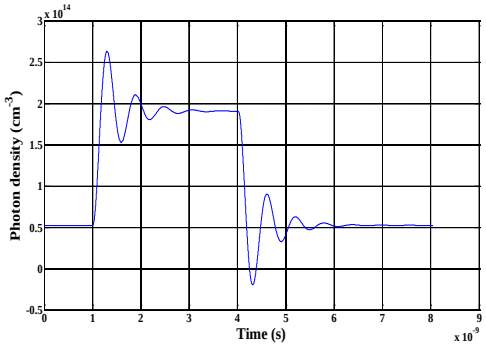

Figure 18: The pulse response of LD1at the bias operating point of 22.1 mA.

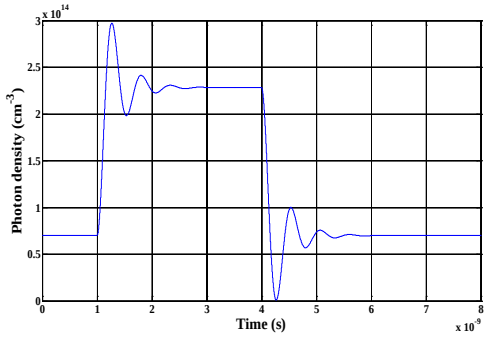

Figure 19: The pulse response of LD2 at the bias operating point of 19.44 mA.

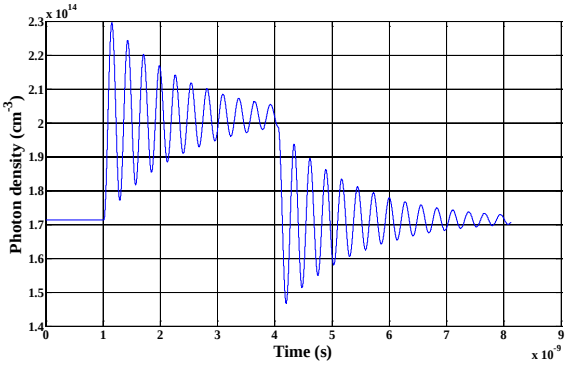

Figure 20: The pulse response of QW-DFB LD at the bias operating point of 15 mA.

The frequency of the RO (f_r) can be calculated according to the following equation [26]:

$$f_r = \frac{1}{2\pi}\left(g_o \frac{S_{on}}{\tau_p}\right)^{\frac{1}{2}} \quad (19)$$

where g_o is the slope gain constant and S_{on} is the first reach steady-state photon density which can be determined from the pulse response as illustrated in Figure 21. Table 4 shows S_{on} and f_r versus the injection current for five pulse responses of LD1 and LD2.

Table 4: The S_{on} and f_r versus injection current for five pulse responses of LD1 and LD2.

LD1			LD2		
Current (mA)	$S_{on} \times 10^{14}$ (cm^{-3})	$f_r \times 10^9$ (Hz)	*Current (mA)*	$S_{on} \times 10^{14}$ (cm^{-3})	$f_r \times 10^9$ (Hz)
17	1.294	2.7	14	1.388	2.701
17.5	1.41	2.823	14.5	1.589	2.89
18	1.498	2.91	15	1.7	2.989
18.5	1.561	2.98	15.5	1.795	3.07
19	1.631	3.036	16	1.858	3.125

Figure 21 shows the frequency of the ROs of LD1 and LD2 as functions of the bias current. It is obvious that the frequency of the RO increases with increasing the bias current. This is due to the increase of the first reach steady-state photon density (S_{on}) with increasing of the bias current as indicated in Eq. (19).

The frequency of the RO of LD2 is slightly higher than that of LD1 because the slope efficiency of LD2 is higher than that of LD1. Consequently, the first reach steady-state photon density of LD2 is higher than that of LD1.

Figure 22 shows the overshoot of the pulse responses versus injection current of LD1 and LD2. The relationship between the overshoot and frequency of RO of the LDs is shown in Figure 23.

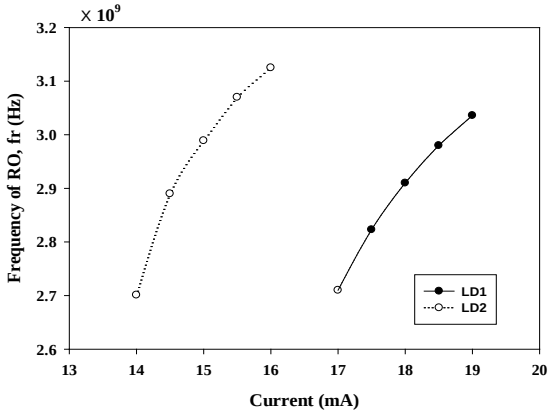

Figure 21: The frequency of ROs as functions of the bias current of LD1 and LD2.

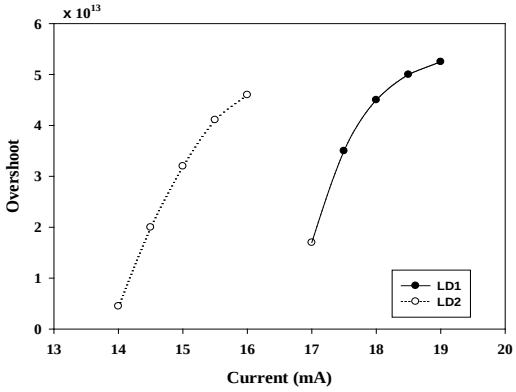

Figure 22: The overshoot of the pulse responses versus injection current of LD1 and LD2.

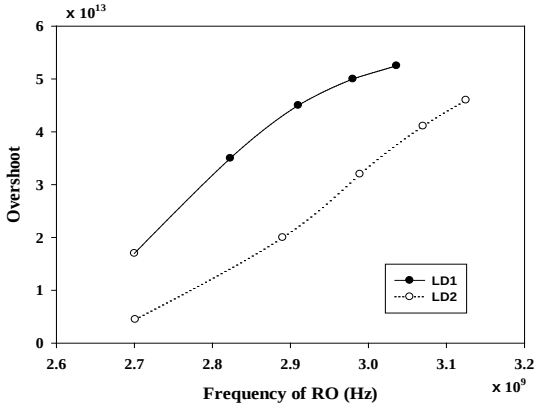

Figure 23: The overshoot versus frequency of RO of LD1 and LD2

6. Bit rate of MQW violet InGaN laser diodes

The damping of the ROs are known to be advantageous for low bit error rate (BER) at large bit rates [27-29]. The present MQW violet InGaN LDs showed a strong damping of ROs on nanosecond scale.

For LD1, Figures (24-26) show the pulse responses at the bias operating point of 17 mA with modulation current of 1 mA above this operating point, and that the duration currents of these pulse responses are 4, 2 and 1 ns, respectively. Figure 24 represents the best pulse response among them, but its bit period is the longest. Figure 25 shows that the bit

period is shorter than that in Figure 24. This means that higher bit rate can be transmitted, but the RO broadens the signal of optical spectrum, thus contributing to an increased BER [30]. Figure 26 shows that the output of the LD1 is severely distorted due to the RO presented in overshoot where the first peak of the RO is almost equal to the duration time (1 ns). Thus, this prevents building of the square wave required for digital modulation which results in a sawtooth like wave.

As for LD2, Figures (27-29) show the pulse responses at the bias operating point of 14 mA with modulation current of 1 mA above this operating point, and that the duration currents of these pulse responses are 4, 2 and 1 ns, respectively.

In terms of modulation, LDs typically convey information for optical communication using either direct or external modulation. In this study, direct modulation has been taken into account. The bit rate (B) is defined as [31]:

$$B = \frac{1}{T_B} \quad (20)$$

where T_B is the bit period. The bit rate of the direct modulation of LD1 and LD2 for the pulse responses 4, 3 and 2 ns are 250, 333.33 and 500 Mb/s, respectively. These values of the bit rate are low compared with the bit rate of the external modulation (> 10 Gb/s) [32]. In fact, the main goal of the external modulation is to reduce or eliminate the RO which results in reducing the bit period then increasing the bit rate. In general, the other type of LDs have almost the same values of the bit rates for direct digital modulation except for VCSEL and QW-DFB LDs in which the bit rate in direct digital modulation have been reported to be more than 10 Gb/s [33, 34]. Figure 30 shows the relationship between the bit rate and the bit period of MQW violet InGaN LDs.

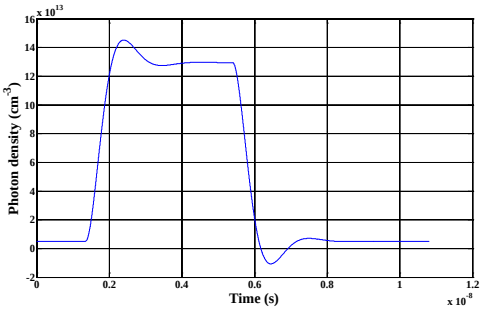

Figure 24: Pulse response to 4 ns with 1 mA modulation current at the bias operating point of 17 mA of LD1.

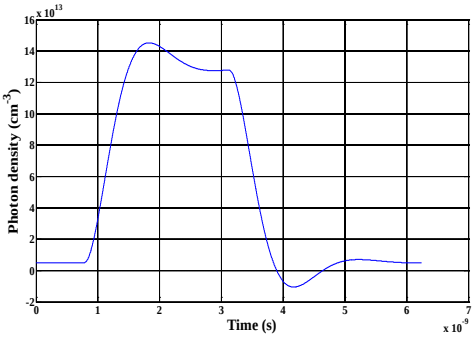

Figure 25: Pulse response to 2 ns with 1mA modulation current at the bias operating point of 17 mA of LD1.

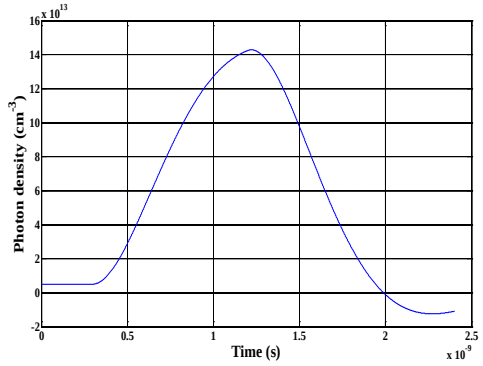

Figure 26: Pulse response to 1 ns with 1 mA modulation current at the bias operating point of 17 mA of LD1.

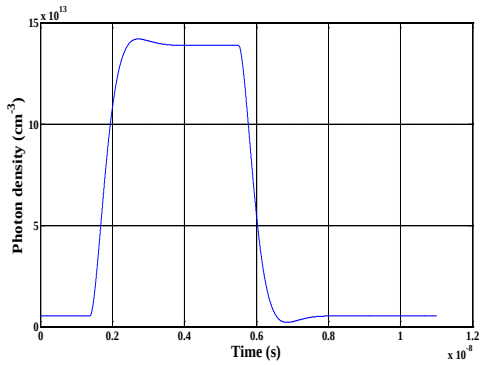

Figure 27: Pulse response to 4 ns with 1 mA modulation current at the bias operating point of 14 mA of LD2.

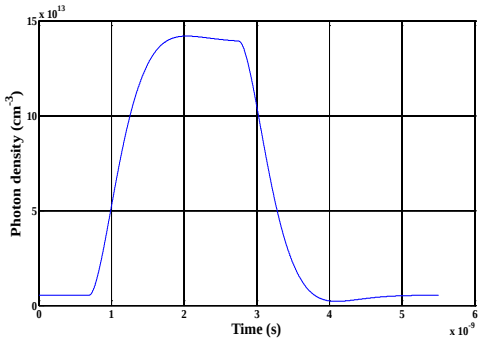

Figure 28: Pulse response to 2 ns with 1mA modulation current at the bias operating point of 14 mA of LD2.

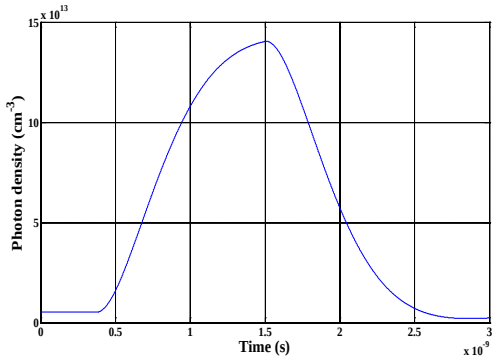

Figure 29: Pulse response to 1 ns with 1 mA modulation current at the bias operating point of 14 mA of LD2.

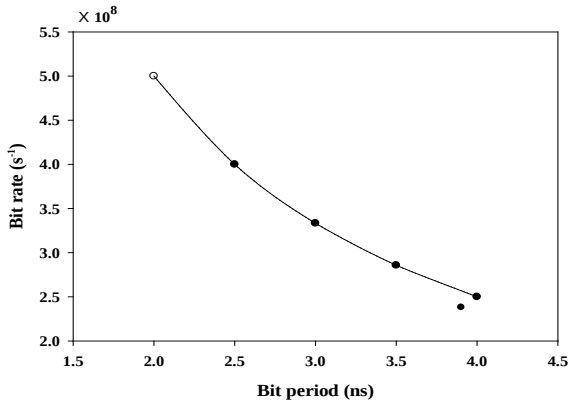

Figure 30: The relationship between the bit rate and the bit period of MQW violet InGaN LDs.

7. Turn-on and turn-off times and extinction ratio

Among the important parameters to be calculated for digital modulation are the turn-on and turn-off times and extinction ratio. Figure 31 shows turn-on and turn-off times of LD1 and LD2 as functions of the bias current. Turn-on and turn-off times represented in Figure 31 are calculated from Figures (7-11) for LD1 and from Figures (13-17) for LD2. As it can be seen from Figure 31, turn-on and turn-off times decrease with increasing of the injection current. This is due to the increase of the frequency of RO [35] with increasing of the injection current. Hence, it is suitable to plot turn-on and turn-off times as functions of the frequency of RO of LD1 and LD2. Figure 32 shows how turn-on and turn-off times change with frequency of RO of LD1 and LD2.

Another important parameter to be calculated is the extinction ratio. The value of extinction ratio is expected to affect turn-on and turn-off time values. Figure 33 represents the extinction ratio as a function of the injection current; the extinction ratio has been taken in (dB) unit because it is more common to measure the extinction ratio. It is obvious that extinction ratio decreases with increasing of the injection current due to the increase of the RO with increasing of the injection current.

In the ideal case, the zero bit optical power is zero which results in an extinction ratio of infinity. In practice, this is not achievable and when the extinction ratio decreases, the difference between zero bit and one bit average optical power decreases. This results in sensitive degradation and a higher probability to mistake zero bits for one bits (or vice versa) resulting in bit errors [36]. Therefore, the power penalty ($\delta_e(r_e)$) is expected to increase with decreasing the extinction ratio as indicated in Figure 34 and according to the following equation:

$$\delta_e(r_e) = \frac{r_e + 1}{r_e - 1} \quad (21)$$

To compare between LD1 and LD2, turn-on and turn-off times are calculated for both of them at the selected operating points above the threshold with 1 mA, i.e. at 17.42 and 14.76 mA for LD1 and LD2, respectively. Turn-on and turn-off times at the selected operating point at 17.42 mA of LD1 were found to be 0.484 and 0.522 ns, respectively; turn-on and turn-off times at selected operating point at 14.67 mA of LD2 were found to be 0.4 and 0.46 ns, respectively. These differences between turn-on and turn-off times of LD1 and LD2 are attributed to the difference of the frequency of the ROs of LD1 and LD2 as indicted in Figure 22 where the frequency of the RO of the LD2 is higher than that of LD1. Turn-on and turn-off times of LD2 are lower than turn-on and turn-off times of LD1 because turn-on and turn-off times are inversely proportional with the frequency of RO as indicted in Figure 32.

In addition, the extinction ratio of LD1 at 17.42 and of LD2 at 14.67 mA are 10.6 and 11.6 dB, respectively. This is another reason to make the turn-on and turn-off times of LD2 lower than those of LD1 as argued above.

Therefore, LD2 is better than the LD1 because LD2 exhibits lower turn-on and turn-off times and higher extinction ratio which means a faster digital communication can be achieved with LD2.

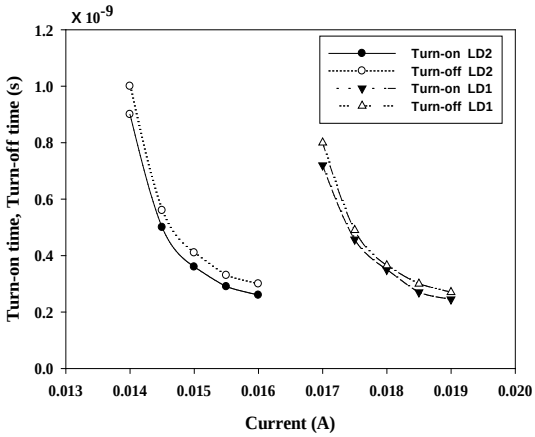

Figure 31: The turn-on and turn-off times as functions of bias current of the LD1 and LD2

.

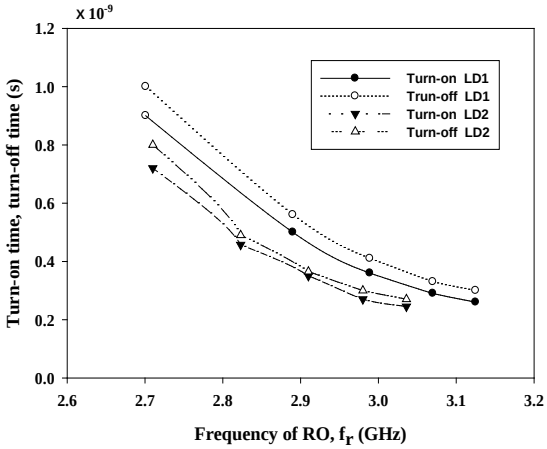

Figure 32: The turn-on and turn-off times as functions of the frequency of RO of LD1 and LD2.

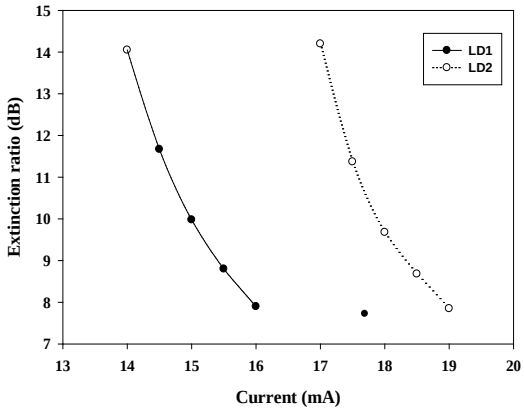

Figure 33: Extinction ratio as a function of the injection current of LD1 and LD2.

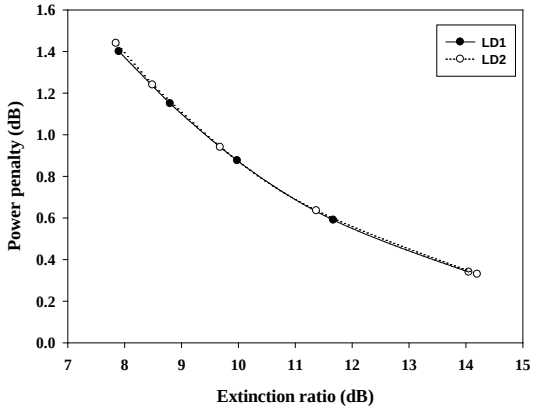

Figure 34: The power penalty as a function of extinction ratio of the LD1 and LD2.

8. Comparison with the Available Experimental Studies

The results of the pulse responses of the MQW violet InGaN LDs have been compared with some available experimental studies.

In term of digital modulation, S. Nakamura et al. have reported 3 GHz frequency of the RO of MQW violet InGaN LD with an emission wavelength near 405 nm [37]. This value is close to the theoretical values of frequencies of the ROs of LD1 and LD2 in this study.

The simulation results indicated that the bit rate in few hundred mega bit per second. This is common in direct digital modulation values of the other LDs. M. Kuramoto et al. modulated three MQW InGaN LDs with the pulse current. They found that the ROs are proportional to the damping constant [38]. Therefore, they concluded that the LD with higher damping constant has a higher RO. This is similar to simulation results in this study where it has been concluded that LD1 has higher RO than LD2 because the damping constant of LD1 is higher than that of LD2.

9. Conclusion

InGaN based-LDs may exhibit better digital modulation characteristic than some conventional LDs. Using AlInGaN BL in nitride based LDs gives good digital modulation characteristics than using conventional AlGaN BL where relatively the fast switching operating can be obtained. The photon and carrier lifetimes of these types of LDs can determine the digital modulation characteristics, designing and fabrication of LDs with appropriate photon and carrier lifetimes can improve their digital modulation characteristics.

References

[1] S. Nakamura, M. Senoh, S. Nagahama, N. Iwasa, T. Yamada, T. Matsushita, H. Kiyoku and Y. Sugimoto, “InGaN-based multi-quantum-well-structure laser diodes,” Jpn. J. Appl. Phys., **35**, L74 (1996).

[2] H. Hirayama, Y. Enomoto, A. Kinoshita, A. Hirata, and Y. Aoyagi, “Room-temperature intense 320 nm band ultraviolet emission from quaternary InAlGaN-based multiple-quantum wells,” Appl. Phys. Lett., **80**, 1589 (2002).

[3] M. Y. Ryu, C. Q. Chen, E. Kuokstis, J. W. Yang, G. Simin, M. Asif Khan, G. G. Sim, and P. W. Yu, “Time-resolved photoluminescence of quaternary AlInGaN-based multiple quantum wells,” Appl. Phys. Lett., **80**, 3943 (2002).

[4] T. Onuma, S. Keller, S. P. DenBaars, J. S. Speck, S. Nakamura, and U. K. Mishra, “Recombination dynamics of a 268 nm emission peak in $Al_{0.53}In_{0.11}Ga_{0.36}N/Al_{0.58}In_{0.02}Ga_{0.40}N$ multiple quantum wells,” Appl. Phys. Lett., **88**, 111912 (2006).

[5] Y. Liu, T. Egawa, H. Ishikawa, B. Zhang, and M. Hao “Influence of growth temperature on quaternary AlInGaN epilayers for ultraviolet emission grown by metalorganic chemical vapor deposition,” Jpn. J. Appl. Phys., **43**, 2414 (2004).

[6] M. Y. Ryu, C. Q Chen, E. Kuokstis, J. W. Yang, G. Simin, and M. Asif Khan, “Luminescence mechanisms in quaternary $Al_xIn_yGa_{1-x-y}N$ materials,” Appl. Phys. Lett., **80**, 3730 (2002).

[7] J. R. Chen, C. H. Lee, T. S. Ko, Y. A. Chang, T. C. Lu, H. C. Kuo, Y. K. Kuo, and S. C. Wang, “Effects of built-in polarization and carrier overflow on InGaN quantum-well lasers with electronic blocking layers,” IEEE J. Lightwave Technol., **26**, 329 (2008).

[8] S. H. Park, H. M. Kim, and D. Ahn, “Optical gain in GaN quantum well lasers with quaternary AlInGaN barriers,” Jpn. J. Appl. Phys., **44**, 7460 (2005).

[9] C. Skierbiszewski, M. Siekacz, P. Wisniewski, P. Perlin, A. Feduniewicz-Zmuda, G. Cywinski, J. Smalc, S. Grzanka, I. Grzegory, M. Leszczynski, and S. Porowski, “High power continuous wave blue InAlGaN laser diodes made by plasma assisted MBE,” ACTA Physica Polonica A, **110**, 345 (2006).

[10] Wei Yang, Ding Li, Juan He and Xiaodong Hu, “Advantage of tapered and graded AlGaN electron blocking layer in InGaN-based blue laser diodes,” Physica status solidi (c), 10, 346 (2013).

[11] S. Nakamura, "InGaN multiquantum-well-structure laser diodes with GaN-AlGaN modulation-doped strained-layer superlattice," IEEE J. Selected Top. Quantum Electron., **4**, 483 (1998).
[12] M. Kuramoto, Y. Hisanaga, A. Kimura, N. Futagawa, A. A. Yamaguchi, M. Nido, and Mizuta, "An alloy semiconductor systems with a tailorable band-tail and its application to high-performance laser operation: II. Experimental study on InGaN MQW laser for optimization of differential gain characteristics tuned by In composition fluctuation," Semicond. Sci. Technol., **9**, 770 (2001).
[13] S. Nakamura, M. Senoh, S. Nagahama, N. Iwasa, T. Yamada, T. Matsushita, Y. Sugimoto, and H. Kiyoku, "Longitudinal mode spectra and ultrashort pulse generation of InGaN multiquantumn well structure laser diodes," Appl. Phys. Lett., **70**, 616 (1997).
[14] L. Bjerkan, A. Royset, L. Hafskjaer, and D. Myher, "Measurement of laser parameters for simulation of high-speed fiberoptic systems," IEEE J. Lightwave Technol., **14**, 839 (1996).
[15] F. Habibullah and W. P. Huang, "A self-consistent analysis of semiconductor laser rate equations for system simulation purpose," Optics Communications, **258**, 230 (2006).
[16] S. Nadarajah, X. N. Fernando, and R. Sedaghat, "Adaptive digital predistortion of laser diode nonlinearity for wireless applications, " IEEE, Montreal, (2003).
[17] Schaer, T. ; Rusnov, R. ; Eagle, S. ; Jastrebski, J , "A dynamic simulation model for semiconductor laser diodes," Electrical and Computer Engineering, IEEE CCECE. Canadian Conference, **1**, 293 (2003).
[18] S. Nakamura, M. Senoh, S. Nagahama, N. Iwasa, T. Matsushita, and T. Mukai, "Blue InGaN-based laser diodes with an emission wavelength of 450 nm," Appl. Phys. Lett., **76**, 22 (2000).
[19] S. Nakamura, "Blue light emitting laser diodes," Thin Solid Films, **343-344**, 345 (1999).
[20] S. Nakamura, M. Senoh, S. Nagahama, N. Iwasa, T. Yamada, T. Matsushita, H. Kiyoku, Y. Sugimoto, T. Kozaki, H. Umemoto, M. Sano, and K. Chocho, "InGaN/GaN/AlGaN-based laser diodes grown on GaN substrates with a fundamental transverse mode," Jpn. J. Appl. Phys., **37**, L1020 (1998).
[21] C. Yuan, T. Salagaj, A. Gurary, A. G. Thompson, W. Kroll, R. A. Stall, C.-Y. Huang, M. Schurman, Y. Li, W. E. Mayo, Y. Lu, S. Krishnamkutty, I. K. Shmagin, R. M. Kolbas, and S. J. Pearton, "Investigation of n- and p-type doping of GaN during epitaxial growth in a mass production scale multiwafer-rotating-disk reactor," J. Vac. Sci. Technol. B, **13**, 2075 (1995).
[22] D. Verhulst, Y. C. Yi, J. Bauwelinck, X. Z. Qiu, S. Verschuere, Z. Lou, and J. Vandewege, "Theoretical and experimental study of laser turn-on delay in a GigaPON system with pre-biasing bits," Proc. Symp. IEEE/LEOS Benelux Cheaper, Amsterdam, (2002).
[23] K. Daikoku, "Direct modulation characteristics of semiconductor laser diodes," Jpn. J. Appl. Phys., **16**, 117 (1977).
[24] M. Fukuda, "Optical semiconductor devices," John & Sons. Inc, New York, (1999).
[25] K. Y. Lau, N. Bar-Chaim, and I. Ury, "Direct amplitude modulation of short cavity GaAs lasers up to X-band frequencies," Appl., Phys., Lett., **43**, 1 (1983).
[26] K. T. Tan, C. Marinelli, M. G. Thompson, A. Wonfor, M. Silver, R. L. Sellin, R. V. Penty, I. H. White, M. Kuntz, M. Lämmlin, N. N. Ledentsov, D. Bimberg, A. E. Zhukov, V. M. Ustinov, and A. R. Kovsh, "High bit rate and elevated temperature data transmission using InGaAs quantum-dot lasers," IEEE Photon. Technol. Lett., **16**, 1415 (2004).
[27] E. Malic, M. J. P. Bormann, P. Hovel, M. Kuntz, D. Bimberg, A. Knorr, and E. Scholl, "Coulomb damped relaxation oscillations in semiconductor quantum dot lasers," IEEE J. Selected Top. Quantum Electron., **13**, 1242 (2007).
[28] M. Kuntz, G. Fiol, M. Lammlin, C. Schubert, A. R. Kovsh, A. Jacob, A. Umbach, and D. Bimberg, "10 Gbit/s data modulation using 1.3 µm InGaAs quantum dot lasers," Electron. Lett., **41**, 244 (2005).
[29] L. Illing and M. B. Kennel, "Shaping current waveforms for direct modulation of semiconductor lasers," IEEE J. Quantum Electron., **40**, 445 (2004).
[30] B. P. Lathi, "Modern digital and analog communication system," Oxford University Press, Inc., (2005).
[31] L. Illing and M. B. Kennel, "Shaping current waveforms for direct modulation of semiconductor lasers," IEEE J. Quantum Electron., **40**, 445 (2004).
[32] A. Ramakrishnan, G. Steinle, D. Supper, C. Degen and G. Ebbinghaus, "Electrically pumped 10 Gbit/s MOVPE-grown monolithic 1.3 µm VCSEL with GaInNAs active region," Electron. Lett., **38**, 322 (2002).
[33] K. Takagi, S. Shirai, Y. Tatsuoka, C. Watatani, T. Ota, T. Takiguchi, T. Aoyagi, T. Nishimura, and N. Tomita, "120 ^{o}C 10-Gb/s uncooled direct modulated 1.3-µm AlGaInAs MQW DFB laser diodes," IEEE Photon. Technol. Lett., **16**, 2415 (2004).
[34] R. S. Tucker, "Large-signal switching transients in index-guided semiconductor lasers," Electron. Lett., **20**, 802 (1984).
[35] B. Chomycz, "Planning fiber optic network," McCraw-Hill Companies, Inc, USA, (2009).
[36] S. Nakamura, M. Senoh, S. Nagahama, N. Iwasa, T. Yamada, T. Matsushita, Y. Sugimoto, and H. Kiyoku, "Longitudinal mode spectra and ultrashort pulse generation of InGaN multiquantumn well structure laser diodes," Appl. Phys. Lett., **70**, 616 (1997).
[37] M. Kuramoto, Y. Hisanaga, A. Kimura, N. Futagawa, A. A. Yamaguchi, M. Nido, and Mizuta, "An alloy semiconductor systems with a tailorable band-tail and its application to high-performance laser operation: II. Experimental study on InGaN MQW laser for optimization of differential gain characteristics tuned by In composition fluctuation," Semicond. Sci. Technol., **9**, 770 (2001).